PHYSICAL REVIEW B VOLUME 50, NUMBER 20 15 NOVEMBER 1994-II

Calculations of the spin dependence of transport and optical properties in wide parabolic quantum wells

C. E. Hembree, B. A. Mason, J. T. Kwiatkowski, and J. E. Furneaux
Department of Physics and Astronomy and Laboratory for the Electronic Properties of Materials, University of Oklahoma, Norman, Oklahoma 73019

J. A. Slinkman
IBM General Technology Division, Essex Junction, Vermont 05452

(Received 28 June 1994)

We use self-consistent solutions to Schrödinger's and Poisson's equations to calculate several observable characteristics of wide parabolic quantum wells in a perpendicular magnetic field. We calculate the dc magnetoconductivity, optical absorption, and acceptor photoluminescence of electrons in these wells. Spin effects are included in both the bare interaction with the magnetic field and the many-body interactions through a local-spin-density exchange-correlation potential. We find several observable signatures of spin effects, enhanced by many-body interactions, in both the magnetotransport and the optical properties of these wells. These include disappearance of integer quantum Hall effect minima in the resistivity, spin polarization, magnetic depopulation of states, and nonlinear Landau fan diagrams. We relate details of these observable phenomena to their microscopic origins in these systems.

I. INTRODUCTION

Wide parabolic quantum wells (WPQW's) are studied because of the homogeneous distribution of the electron gas in such structures and the intermediate dimensionality between two-dimensional (2D) and three-dimensional (3D) physics. The electron gas, in screening the parabolic conduction band edge potential, forms a constant density slab, an approximation to *jellium* where electrons move in a constant positive background charge density. The nearly complete screening of the external potential, and the resultant wide, flat potential well, causes the exchange and correlation terms in the electron-electron interaction to be very important to the observable properties of the well. When placed in a magnetic field, the spin of the electrons can strongly influence the exchange-correlation energy of the electron gas. The large width of the wells and resultant small subband spacing make them ideal for studying these spin effects.

Since the first realization of wide parabolic quantum wells through molecular beam epitaxy growth,[1] there have been significant studies of this system, both experimental and theoretical. Much of the experimental work has been on either magnetotransport[2–4] or infrared studies.[5,6] These have confirmed the parabolic nature of the well, and shown the exact renormalization of the subband spacing in long wavelength optical absorption.[7] More recently, significant work has been performed on capacitance,[8] and photoluminescence[9] in these wells. In theoretical studies, several researchers have calculated the subband spectrum of these wells,[10–14] including perpendicular, parallel, and tilted magnetic fields, variations in the effective mass across the well, and symmetry breaking potential structures on top of the parabolic potential. This work has shown interesting properties of the infrared absorption, magnetotransport, and possible correlated electron states in these wells.

In a recent paper,[14] we investigated the effect of spin on the subband spectrum in these wells. We considered a well in a perpendicular magnetic field, and included the electron spin through both the bare g factor and a spin-dependent exchange-correlation potential within the local-spin-density approximation (LSDA).[15,16] This LSDA gives an effective potential that depends on the local density and spin polarization of the electron gas. The spin effects were included self-consistently in the subband spectrum calculation. We found that the electron gas can undergo significant changes due to the spin. In many wells, the electron gas will undergo an abrupt spin polarization with increasing magnetic field. Due to the closely spaced subband levels, the enhancement of the effective g factor can cause the spin energy to become larger than the intersubband spacing, resulting in the population of only one spin level and several subbands. We also found spin density waves across the width of the well and a sign change of the effective g factor for the lowest electron subband for certain magnetic field values and well geometries.

In this paper, we will consider observable signatures of the spin effects described previously. In particular, we are interested in the spin polarization of the electron gas and enhancements of the effective g factor. We study $Al_xGa_{1-x}As$ systems with the Al concentration tailored to produce a parabolic conduction band minimum.[1] These MBE grown wells are populated via remote Si doping layers. The well is characterized by its width, curvature, and filling factor f where f is given by

$$f = \frac{n_2}{n_3 w}. \tag{1}$$

0163-1829/94/50(20)/15197(13)/$06.00

n_2 is the 2D sheet density and w is the width of the parabolic well. n_3 is the constant 3D density of background positive charge that will give the same potential as the graded $Al_xGa_{1-x}As$ structure. n_3 is sometimes called the "target density" of the well and is determined by the curvature of the conduction band edge. We use the eigensolver described in our previous papers[13,14] to calculate the eigenenergies and wave functions of electrons in a WPQW. This eigensolver employs a fourth-order Runga-Kutta integration and a self-consistent iteration scheme similar to those used by other researchers.[17,10,12] These, in turn, are used to obtain the magnetotransport spectra, the infrared absorption (σ_{zz}), and the acceptor photoluminescence strength of the well. In all of this work, we consider the geometry where there is a magnetic field perpendicular to the plane of the 2D electron gas. The finite potential walls bounding the parabolic potential are included along with a phenomenological broadening of the electron states. We do not include temperature because the impurity broadening of the electronic states is larger than k_BT. We have also assumed the electronic conduction band is parabolic at energies less than 10 meV of interest in this paper, and have not considered the effective mass dependence on the changing Al concentration across the well.

The organization of the paper is as follows. In Sec. II, we calculate the magnetotransport at arbitrary magnetic fields in parabolic wells. We find that transport in low magnetic fields is relatively insensitive to field-dependent many-body effects. At higher fields, the exchange-correlation enhancement of the spin splitting is important for understanding the quantum Hall spectrum. In Sec. III, we compute the infrared absorption of full or nearly full wells. The hard walls of the well allow us to see features beyond the single center-of-mass mode. We see features of the photoabsorption that can be associated with subband depopulation and the spin polarization. In Sec. IV, we compute the optical matrix elements of acceptor photoluminescence in parabolic wells. The photoluminescence spectrum mirrors the subband structure including nonlinearities in the energy levels with changing magnetic field, spin splitting, and polarization. Section V is a brief summary of our results.

II. MAGNETOTRANSPORT

Magnetotransport measurements have revealed interesting features in WPQW samples. Ensslin and coworkers[4] found that quantum Hall plateaus disappear and reappear as a function of the 2D density, n_2, in the well. This phenomena is better observed via the minima in the longitudinal resistivity, ρ_{xx}, that disappear and reappear in concert with the Hall plateaus. Here, we present results of calculations of the magnetotransport spectrum in these wells that agree with experimental results. We find that spin splitting plays a substantial role in determining the densities where this occurs. Additionally, we show that an abrupt spin polarization of the electron gas might be observable via transport measurements.

To generate the conductivities and, hence, the resistivities, it is first necessary to calculate the density of states. For magnetotransport in two dimensions, this depends on two factors, the energy level structure of the electron system and the broadening of levels due to scattering. Scattering is taken into account in our model by considering an *ad hoc* field-independent broadening of each energy level. The broadening function is given by a truncated Lorentzian:

$$F(x) = N\left(\frac{1}{x^2+\Gamma^2} - \frac{1}{17\Gamma^2}\right), \quad |x| \le 4\Gamma \qquad (2)$$
$$= 0, \quad |x| > 4\Gamma,$$

where N is a normalization constant,

$$\int_{-4\Gamma}^{4\Gamma} F(x)dx = 1. \qquad (3)$$

In this approximation, the total density of states is given by

$$g(E) = \sum_{i,n,s} N_l F(E - E_{i,n,s}), \qquad (4)$$

where $E_{i,n,s}$ are the self-consistent eigenenergies of Schrödinger's equation for subband i, Landau level n, and spin s. N_l is the 2D density of a filled Landau level. Γ, the level broadening, is assumed to be the inverse of the transport scattering time. This level broadening is included in the self-consistent LSDA calculation of the states.

The form that we use for the broadening is an approximate description of the constant, short range scattering from the Al alloy in the well. For the range of magnetic fields and densities of interest here (around $\nu = 4$), this field-independent level broadening shows the best agreement with experiment of several broadening functions we investigated. To a large extent, the energy level spectrum is insensitive to the shape of the broadening. However, we have found that the shape of the broadening function does effect the transport properties. A positive curvature for the tails of the density of states peaks of each Landau level, such as in Eq. (2) above, is necessary for agreement with experimental results. We found that the behavior of the $\nu = 3$ minima observed by Ensslin *et al.*[4] did not appear when we used a field-dependent broadening such as the standard self-consistent Born model.[18] The broadening of the levels increased faster than the spacing between the spin levels as the density was increased. Thus the $\nu = 3$ plateau does not appear at all in this system with the self-consistent Born density of states. At high magnetic fields, we expect the self-consistent Born approximation due to ionized impurities to hold. This would give an elliptical broadening proportional to the square root of the magnetic field.

We calculate the magnetoconductivity from[19]

$$\sigma_{xx} = \frac{\sigma_0}{1+\omega_c{}^2\tau^2} + \frac{\sigma_0}{1+\omega_c{}^2\tau^2}\frac{\Delta g_F(B)}{g_F(0)}, \qquad (5)$$

$$\sigma_{xy} = \frac{\sigma_0}{1+\omega_c{}^2\tau^2}\omega_c\tau - \frac{\sigma_0}{1+\omega_c{}^2\tau^2}\frac{1}{\omega_c\tau}\frac{\Delta g_F(B)}{g_F(0)}, \qquad (6)$$

where $\omega_c = eB/m^*c$ is the cyclotron frequency, $\sigma_0 = N_0 e^2\tau/m^*$ is the classical zero field conductivity, $\tau = 2\hbar/\Gamma$ is the transport scattering time derived from the experimental mobility, and $\Delta g_F(B) = g_F(B) - g_F(0) = g(E_F;B) - g(E_F;0)$ is the magnetic field induced change in the density of states at the Fermi energy. The resistivity is determined by inverting the 2D conductivity tensor. We calculate both the low field Shubnikov–de Haas (SDH) and high field quantum Hall effect magnetoresistivity.

Measurements of the low field SDH spectrum of quantum wells are often compared to a "rigid potential model" for the subbands in standard 2D electron gas systems. In this model, the subband energies are determined at $B = 0$, and then Landau levels are extended linearly from these energies. As has been pointed out by several researchers,[10,13] this is not a good approximation in wide parabolic wells. It ignores the field-dependent exchange-correlation effects seen in the fully self-consistent calculations. However, it turns out that the SDH spectrum agrees quite well with the rigid potential model, even though the subband spectrum is quite nonlinear.

Figure 1 compares the fully self-consistent SDH spectrum to this linear subband approximation. Figure 1(a) is the magnetoresistivity, ρ_{xx}, plotted as a function of field. Figure 1(b) is the Fourier transform of the resistivity giving approximate population of states. One sees that the two are essentially indistinguishable. This is due to the fact that, at low fields, the spacing between Landau levels is much smaller than the broadened width of the levels. This leads to a relatively smooth density of states which allows the Fermi energy to remain almost constant as a function of magnetic field. Therefore, the relative populations of the different subbands also tend to remain constant leading to a rigid potential type of behavior of the SDH spectrum. Shubnikov–de Haas simply counts electrons in each state and the nonlinearities in the subband energies will not be observed. The inclusion of the broadening of the self-consistent states is necessary to understand this agreement. Without broadening, we find that both the subbands and E_F are highly nonlinear functions of the magnetic field.[13]

It is possible that the spin dependence of the electron gas will have an observable effect on the SDH spectrum in a parabolic quantum well. We have found a signature in the resistivity of an abrupt spin polarization of the electron gas.[14] This polarization causes significant changes in the electronic energy levels, density profiles, and populations. In Fig. 2(a) we show the subband spectrum (lowest Landau level of each subband) as a function of magnetic field. Spin-down levels are plotted with solid lines, spin-up levels are plotted with dashed lines, and E_F is plotted with a dark solid line. Figure 2(b) shows the SDH signal corresponding to this well. At B=3 T, a spin polarization occurs where the electrons abruptly fall into a single spin state with two subbands populated. At this field, we see a spike in the SDH signal due to the change in the population and density of states at E_F. It is unlikely, however, that such a signal could be observed experimentally because it will be washed out by density inhomogeneities across the sample.

At higher magnetic fields, energy level crossings have a profound effect on the transport properties. In Fig. 3 we show the longitudinal resistivity, ρ_{xx}, as a function of field for several different electron densities for a well of width 750 Å and height of the parabolic region of the well of 75 meV, similar to Ennslin *et al.*[4] The 2D densities range from 2.84×10^{11} cm^{-2} to 3.98×10^{11} cm^{-2}. The ρ_{xx} axis is offset for each density graph. Lines have been drawn to show the ν = 2, 3, and 4 minima. We no-

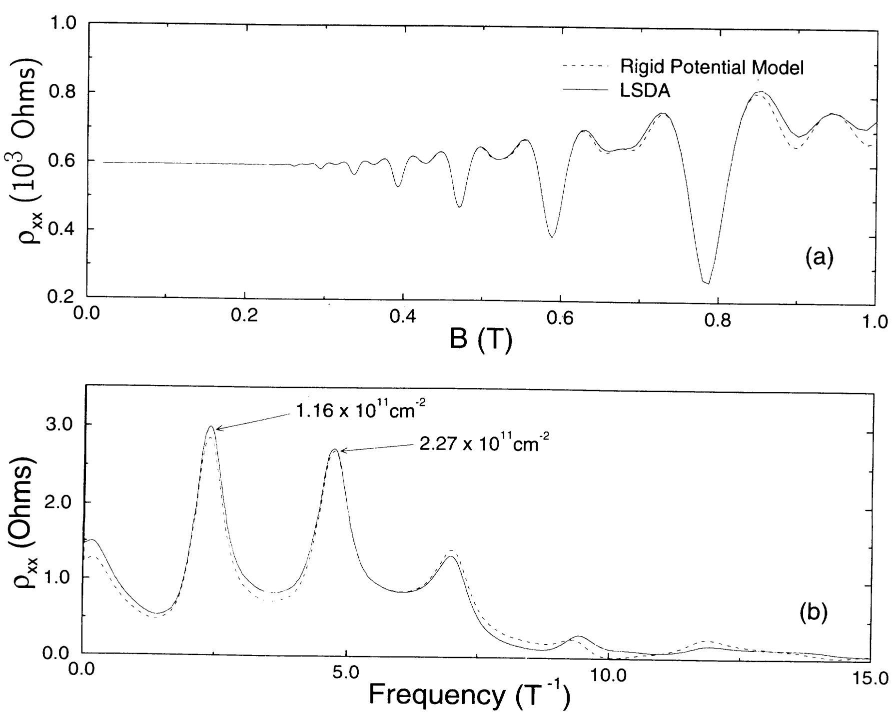

FIG. 1. Magnetoresistance of a wide parabolic quantum well. The solid line is fully self-consistent calculation and the dashed line is rigid potential model. (a) ρ_{xx} vs magnetic field. (b) Shubnikov–de Haas spectrum.

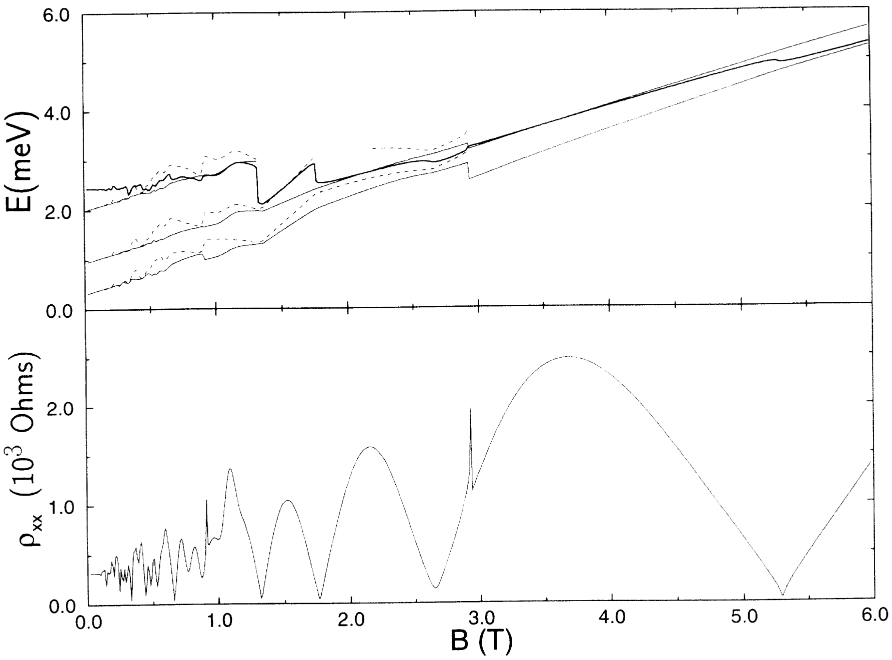

FIG. 2. Subband spectrum (top) and Shubnikov–de Haas spectrum for a quantum well with a spin polarization at $B = 2.9$ T.

tice that for certain values of the 2D density, the $\nu = 4$ minimum disappears in excellent agreement with the experimental results. This occurs when the second Landau level of the first subband crosses the first Landau level of the second subband at the Fermi energy, eliminating the energy gap at E_F. We find that spin plays an important role in the details of the minimum disappearance even though this minimum is usually a Landau level gap rather than a spin gap.

Pronounced minima in ρ_{xx} appear at integer filling factors when E_g, the gap between energy levels at the Fermi energy, is greater than 2Γ. If $E_g < 2\Gamma$, the minimum in ρ_{xx} disappears and also the Hall plateau is suppressed. For field-independent broadening, there are two possible causes for the closing of the gap. There may be a reordering of the electron density and spin that inherently narrows the subband spacing or there may be a level crossing. The behaviors which we observe in the $\nu = 4$ minima in Fig. 3 occur due to both of these effects. In Fig. 4, we show the many-body and spin dependence of this gap. In this figure, we plot the electron energy levels as a function of magnetic field at $\nu = 4$. The density of the electron gas is changed as a function of the magnetic field such that the electron gas remains at $\nu = 4$. The lowest Landau level of the first two subbands are shown as solid lines, the second Landau level of the first subband is shown as a dashed line, and the Fermi energy is shown as a wide solid line. The spin of each state is given by the up or down pointing triangles. We see that at the level crossing, the spin splitting is enhanced by the

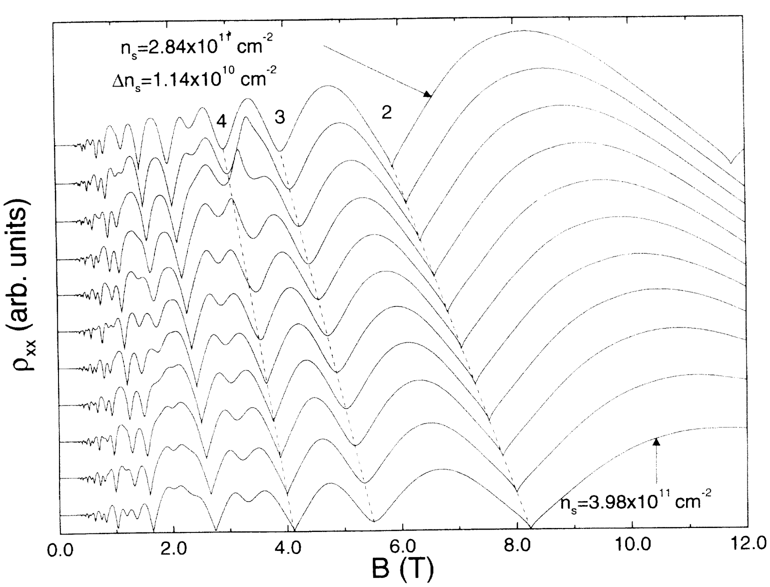

FIG. 3. Magnetoresistance of a wide parabolic quantum well, width $w = 750$ Å and density $n_3 = 7 \times 10^{16}$ cm^{-3}, for different 2D densities. Dashed lines give the $\nu = 2, 3, 4$ quantum Hall minima. Note disappearance and reappearance of the $\nu = 4$ minimum.

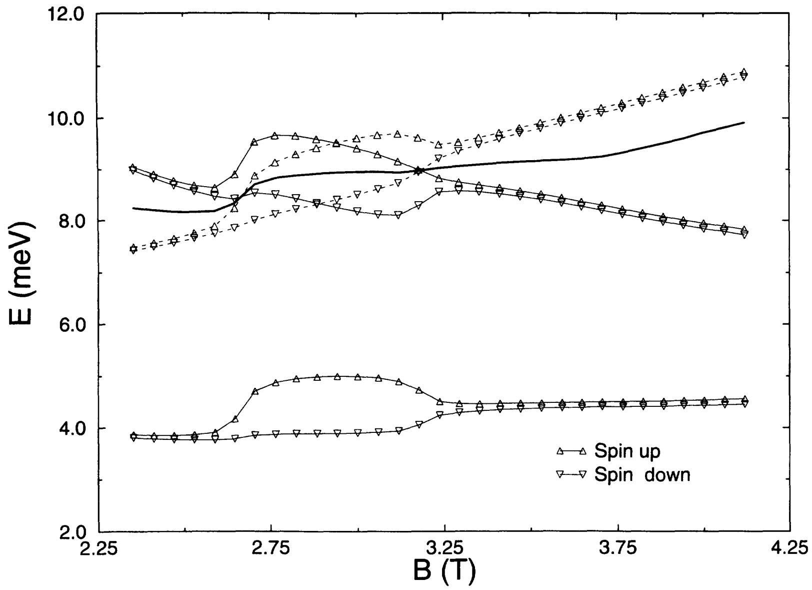

FIG. 4. Subband and Landau level spectrum of same parabolic well as in Fig. 3 for $\nu = 4$ as a function of magnetic field. First Landau level of the first two subbands are narrow solid lines. Second Landau level of the first subband are dashed lines. Fermi energy is thick solid line. The electron spin is indicated by the triangles.

exchange-correlation effects. The lower spin split levels are preferentially populated, changing the Landau level gap to a spin gap. This affects the density and magnetic field ranges where the disappearance of the $\nu = 4$ gap will be seen. Due to the spin splitting, the Fermi level is pinned for a wide range of fields at an energy where there will be a small energy gap. Without the enhanced spin splitting, the levels will cross without such a pinning.[13]

III. OPTICAL ABSORPTION

The infrared intersubband absorption of electrons in wide parabolic wells has received a great deal of attention.[20–23] As pointed out by Brey *et al.*,[7] the absorption of electrons in a perfect parabolic potential will be only at a single frequency, corresponding to the 3D plasma frequency of the electron gas. Experiments have confirmed this result, giving good evidence that the manufactured wells are, indeed, parabolic.[20,21] Adding potential structures to the well that break the parabolic symmetry, such as spikes, superlattices, or the hard side walls of the well,[6,24] allows more detailed optical study of the electron gas. In a recent series of papers, Dempsey and Halperin[25,26] have performed a careful theoretical study of the infrared absorption in these wells without including the effects of the electron spin. In this section, we consider the effects of spin on the optical absorption in quasi-three-dimensional systems.

We follow the development originally used by Ando[27] for 2D electron systems and add the required formalism to treat spin effects. In the following exposition, the ψ's are the one-dimensional wave functions obtained from solving Schrödinger's equation self-consistently along the growth axis of the parabolic quantum well. The calculation of the photoconductivity is performed for the geometry where the applied electric field, $De^{-i\omega t}$, is polarized in the z direction to excite only the intersubband mode and not the cyclotron resonance mode. For the intersubband mode, one expects a strong central peak of the conductivity at $\hbar\omega_p$, independent of magnetic field, for a perfect parabolic well. In this work, we consider nearly full wells, so that deviations from this single "Kohn mode" are due to the hard walls of the well that break the translational invariance of the parabolic potential. We are interested in the deviations of the absorption from this single Kohn mode due to the walls, magnetic depopulation of states, and spin.

The self-consistent states and energies are used to compute the corrections to the bare transition optical matrix elements. The shift to lower frequencies caused by electron-hole interactions takes the form of the vertex (or excitonic) correction:

$$\beta_{k,l;k',l'} = -\int_{-\infty}^{+\infty} \psi_k(z)\psi_l^*(z)\Delta V_{\rm xc}\psi_{k'}(z)\psi_{l'}^*(z)dz, \quad (7)$$

where the change in $V_{\rm xc}$ due to the perturbing field is

$$\Delta V_{\rm xc} = \sum_k \left(\frac{\delta V_{\rm xc}}{\delta n} + 1/n_2\frac{\delta V_{\rm xc}}{\delta \xi}\right)\Delta n_k. \quad (8)$$

The indices, k, l, k', l' label the electronic subband, Landau level, and spin of the self-consistent states. Thus, these are triplet indices, $k \Rightarrow (i_k, l_k, s_k)$. dn_k is the change in electron density for each state. Both density and spin-polarization effects are included in this expression. $\xi(z) = [\rho_+(z)-\rho_-](z)/[\rho_+(z)+\rho_-(z)]$, where $\rho_\pm(z)$ is the local 3D density of the spin-up and spin-down electron gases, is the local polarization of the electron gas. $V_{\rm xc}$ is the spin-dependent LDA exchange-correlation potential.[15,16] It depends on both total density and spin polarization so that

$$\frac{\delta V_{\rm xc}}{\delta\xi}\Delta\xi = \sum_k 1/n_2\frac{\delta V_{\rm xc}}{\delta\xi}\Delta n_k. \quad (9)$$

One should note that the sum in this expression includes a sum over the two spins.

The shift to higher frequencies due to the resonance screening (or depolarization) correction has the form

$$\alpha_{k,l;k',l'} = -\frac{4\pi e^2}{\epsilon}\int_{-\infty}^{+\infty} dz\ \psi_k(z)\psi_l^*(z) \times \int_{-\infty}^{z} dz' \int_{-\infty}^{z'} dz''\ \psi_{k'}(z'')\psi_{l'}^*(z''). \quad (10)$$

These terms are used to calculate the transition matrix:

$$\Lambda_{k,l;k',l'} = E_{k,l}^2\ \delta_{k,k'}\ \delta_{l,l'} + (n_k - n_l)^{1/2}(n_{k'} - n_{l'})^{1/2} \times (E_{k,l}E_{k',l'})^{1/2}(\alpha_{k,l;k',l'} - \beta_{k,l;k',l'}). \quad (11)$$

In this equation, n_k is the 2D density of the state k and $E_{k,l}$ is the energy difference between the states k and l.

The structure of this matrix is key to the calculation. For our computation, we have not included spin flip transitions so that the Λ matrix is divided into four quadrants. The upper left quadrant describes pairs of electrons making $s_k, s_{k'} =\uparrow$ to $s_l, s_{l'} =\uparrow$ transitions. The lower right quadrant describes pairs of electrons making $s_k, s_{k'} =\downarrow$ to $s_l, s_{l'} =\downarrow$ transitions. The off-diagonal quadrants describe $s_k =\uparrow$ to $s_l =\uparrow$ and $s_{k'} =\downarrow$ to $s_{l'} =\downarrow$ transitions, and *vice versa*.

The eigenvalues of this matrix, $\tilde{E}_l^2$, are the squares of the experimentally observed transition energies in the system. The eigenvectors of this matrix are used to construct the oscillator strengths:

$$\tilde{f}_l = \left[\sum_{k,k'}\left(\frac{2m^*}{\hbar^2}(E_{k,k'})\right)^{1/2} Z_{k,k'} \times \left(\frac{n_k - n_{k'}}{n_2}\right)^{1/2} U_{k,k';l}\right]^2, \quad (12)$$

where $U_{k,k';l}$ are the elements of the lth eigenvector of Λ, and $Z_{k,k'}$ are the matrix elements of z between the k and k' states. We use the sum rule on these oscillator strengths to check the calculation and to determine if we are using a sufficiently complete set of states.

Finally, the conductivity is calculated by

$$\sigma_{zz}(\omega) = \frac{e^2}{m^*}(-i\omega)n_2\sum_l \frac{\tilde{f}_l}{\tilde{E}_l^2 - (\hbar\omega)^2 - 2i\hbar\omega/\tau}. \quad (13)$$

We choose our phenomenological relaxation time τ to correspond to the level broadening in the wave function calculation as described in Sec. II above.

We perform the calculations for a parabolic quantum well which is 1000 Å wide and with filling factors of 0.6, 0.8, and 1.0. The Al concentration at the edge of the well is 5% to produce a well depth of the parabolic region of 40 meV. The result is a well with two states at $B = 0$ for the 0.6 and 0.8 filling factor and with three states at $B = 0$ for the 1.0 filling factor. These parameters correspond to a well with a target 3D density of $n_3 = 2.25 \times 10^{16}$ cm^{-3} and a plasma frequency of $\hbar\omega_p = 5.55$ meV. We investigate such a wide, shallow well because of the enhanced exchange-correlation effects and a strong spin polarization.

In Fig. 5, we show the subband spectrum and photoconductivity of the full well (filling factor $f = 1.0$). This well is effectively a square well, the bare parabolic potential canceling the Hartree term in the electron-electron interaction, giving a strong interaction between the electrons and the walls. Figure 5(a) shows the energies of the lowest Landau levels of each of the subbands as a function of the magnetic field (the subband spectrum). Each spin state is shown, with the Fermi energy given by the thick line. Figure 5(b) shows $\log_{10}\sigma_{zz}(\omega)$ as a function of magnetic field and energy. We see strong peaks near the 3D plasma frequency, shifted upwards by the interactions with the walls of the well, and satellite peaks caused by the hard walls of the well. In Fig. 5(c), we plot the contours of $\log_{10}\sigma_{xx}(\omega)$. In Fig. 5(c), the transition energy is the horizontal axis and magnetic field is the vertical axis. There are two very nonlinear peaks that begin, for $B = 0$, at 6.32 and 6.85 meV, and two satellite peaks that disappear due to subband population at 9.74 and 12.4 meV. We should note that satellite peaks above the 3D plasma mode have been observed in tilted field experiments.[21]

The behavior of the conductivity peaks as a function of field has several features of interest. One can determine the physics of these features by comparing the conductivity [Fig. 5(c)] with the subband spectrum [Fig. 5(a)]. The disappearance of the highest energy conductivity peak around 2.3 T corresponds to the depopulation of the third subband in the system. Up to this field, the energy of all the peaks remain constant. Above 2.3 T, the second subband begins to depopulate, with a corresponding decrease in the conductivity peak at 9.74 meV. In this regime of magnetic field, we also see an increase in the splitting between the two main conductivity peaks that reaches a maximum when the second subband is fully depopulated. The two different peaks here correspond to the two spins, because the excitonic correction [(Eqs. (7) and (8)] depends on spin through the spin-dependent exchange-correlation potential and the interaction with the well walls. This is the magnetic field regime where we see a maximum in the spin splitting in the subband spectrum due to V_{xc}. The system undergoes a spin polarization at around 5.5 T. At this field, the energy of the electron gas is minimized by populating only a single spin state. Changes in the exchange-correlation energy and the electron density cause a significant shift in the subband energies of the well, and one spin of the second subband is repopulated. This effect is reflected in the conductivity by the reappearance of the satellite peak at 9.74 meV and the shift back together of the two main conductivity peaks around 6.5 meV. This change in the conductivity is very large because the second subband has an odd parity wave function across the well and thus has peaks near the walls giving a strongly non-parabolic potential term. For fields above the polarization, the satellite conductivity peak again decreases and disappears as the second subband depopulates, and the main peaks again separate with increasing field due to spin-dependent excitonic corrections.

For a system with filling factor $f = 0.8$, we find a subband spectrum with many of the same features as the

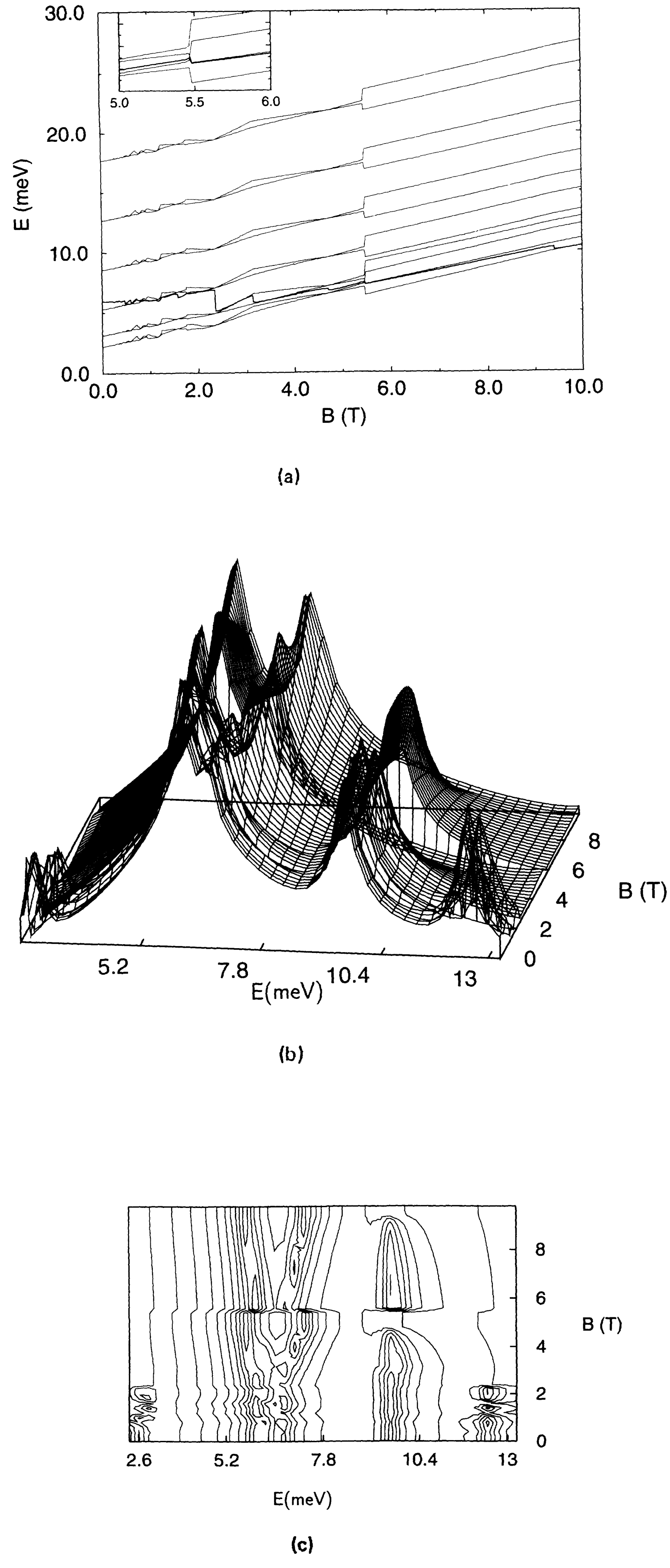

FIG. 5. Infrared optical absorption spectrum of a wide parabolic well, w = 1000 Å and $n_3 = 2 \times 10^{16}$ cm^{-3} at f = 1.0. (a) Subband spectrum as a function of magnetic field, (b) $\log_{10} \sigma_{xx}(\omega)$ as a function of energy and magnetic field, (c) Contour plot of $\log_{10} \sigma_{xx}(\omega)$.

full well. This is plotted in Fig. 6(a), with $\log_{10}\sigma_{xx}(\omega)$ shown in Figs. 6(b) and 6(c). There is a single satellite peak, at 10.0 meV, that disappears with field corresponding to the second subband in the well. Because there is less overlap between the electron wave functions and the walls, the Kohn mode is a more dominant feature in the conductivity with a strong, relatively constant peak at 5.79 meV and a much smaller spin-split peak at 7.37 meV. This is again above the 3D plasma frequency, but is much closer than for the full well. Because we are plotting $\log_{10}\sigma_{xx}$, the peaks at 7.37 meV and 10.0 meV in this figure are more than an order of magnitude smaller than the main peak. A spin polarization also occurs in this system at a magnetic field of 5.5 T but the effects on the subband energies are clearly smaller. The satellite peak at 10.0 meV reappears only slightly at the spin polarization. This is because the second subband is only partially repopulated by the polarization and is quickly depopulated with increasing magnetic field. Above 7.5 T, where there is only a single state filled and the conductivity is constant reflecting the constant subband spacing.

The above results can be contrasted to results from a system with $f = 0.6$ shown in Fig. 7. Here, the satellite conductivity peaks are five orders of magnitude smaller than the Kohn mode, and the main conductivity peak does not change position as a function of magnetic field. This is due to the separation of the populated wave functions in the well and the hard walls at the edge of the well. This system acts like an infinite parabolic system.

Our results show the effects of spin on the absorption spectra in these wells when the electrons interact with the hard walls. The walls cause satellite peaks in the conductivity corresponding to higher populated subbands. There is also splitting of the Kohn mode due to the spin dependence of the exchange-correlation potential when the electrons interact with the well walls. The satellite peaks generally disappear as the magnetic field is increased and the subbands depopulate, one spin at a time. The peaks can grow and shift significantly at high fields when the spin effects in the exchange-correlation potential become large. This is particularly noticeable when the system undergoes a spin polarization and repopulates higher subbands. These effects will give observable signatures of the spin polarization.

IV. ACCEPTOR PHOTOLUMINESCENCE

Photoluminescence spectroscopy in wide parabolic quantum wells will reveal details of the subband structure that cannot be determined by other experimental means. Because the interaction between the optical hole and the electron gas breaks the translational symmetry of the problem, this experiment will not be limited by Kohn's theorem to observe simply the bare, 3D plasma frequency. Details of the subband energies will be observable, including nonlinearities of the subband spectrum, enhanced spin splitting, and spin polarization. Fritze and co-workers and Burnett *et al.*[9] have performed luminescence experiments in wide parabolic quantum wells where they have observed free exciton transitions. They have found nonlinear spectra as a function of increasing magnetic field, in good qualitative agreement with our previous work.[13]

In this section, we study the optical transitions between the electrons confined in the parabolic quantum well and holes bound on acceptor levels. We assume the parabolic well is lightly doped at its center with a δ layer of acceptors (Be or Zn, e.g.) and consider luminescence due to transitions from the quasi-three-dimensional electron gas to the ground state of the bound acceptor levels. Assuming the doping is low enough to neglect correlations between acceptors, we consider only a single acceptor. Because of the strength of the interaction between the electron gas and the bound hole, there will be a strong, distinguishable signal from a lightly doped δ layer. Acceptor luminescence experiments have several advantages over those involving free exciton transitions. The transition to a single energy level gives a sharper energy spectrum due to the bound state of the optical hole. The large acceptor binding energy in GaAs, 30 meV for Be, implies that there is a single, well defined final state for the electron after transition. The luminescence energy will be distinct from transitions across the band gap and the pumping radiation. This well defined hole state also has the advantage of being spatially localized, giving distinctly different transition probabilities for different electron subbands, the transition being roughly proportional to the magnitude of the electron probability density at the acceptor site. In the case of doping at the center of a symmetric well, there will be transitions only from even parity states. Doping the well at different places will give different information about the bound states of the electrons. Before the transition, the bound hole-acceptor state is neutral, causing little change in the initial electronic states of the well. Finally, because the ground acceptor state is, to a very good approximation, heavy-hole like, there will be a distinct polarization dependence to the transitions. This will allow the observation of electron spin effects in the parabolic well.

We have calculated the optical transition matrix elements within Fermi's golden rule. In this approximation, the emission rate has the form

$$R_{i,n,m,s}(E_{\mathrm{phot}}) \propto \frac{1}{{E_{\mathrm{phot}}}^2}|\langle a|\hat{\mathbf{P}}\cdot\boldsymbol{\epsilon}|i,n,m,s\rangle|^2 \times\delta(E_a - E_{i,n,s} + E_{\mathrm{phot}}). \tag{14}$$

In this expression, E_{phot} is the energy of the luminescence, $\boldsymbol{\epsilon}$ is the polarization of the luminescence, and $\hat{\mathbf{P}}$ is the momentum operator of the electron. The electronic states and energies are $\{|a\rangle,\ E_a\}$, the acceptor level, and $\{|i,n,m,s\rangle,\ E_{i,n,s}\}$, the conduction band state for an electron in the subband i, Landau level $\{n,m\}$ where we use the symmetric gauge to describe the external magnetic field (n is the Landau level number and m labels the degenerate states within a Landau level), and spin s. Using the form of the density of states described in Sec. II above, the total emission spectrum for the luminescence has the form

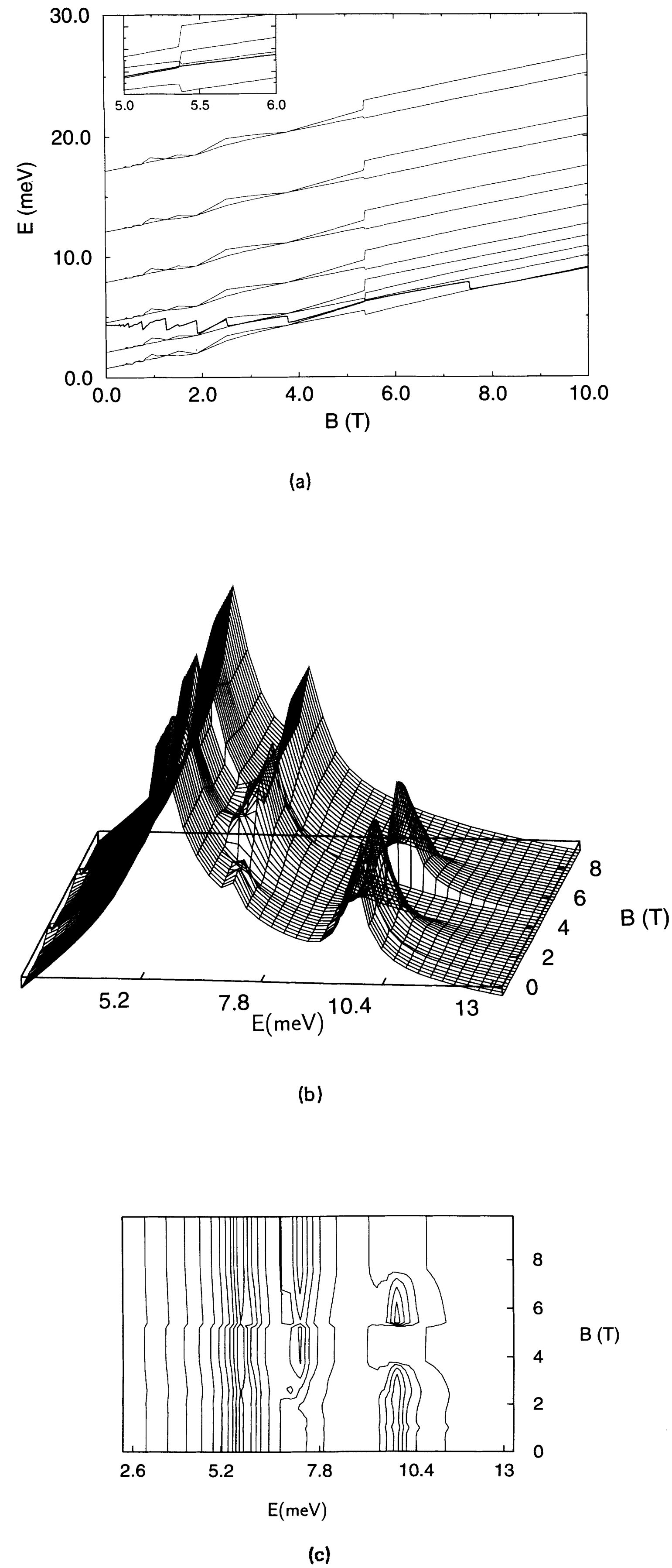

FIG. 6. Same as Fig. 5 with $f = 0.8$.

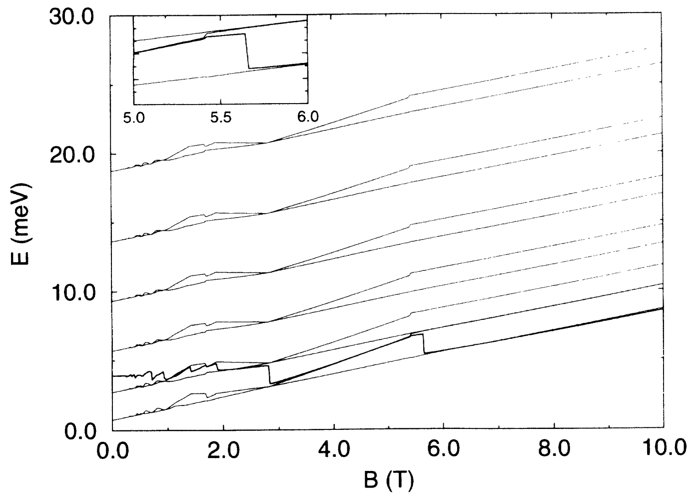

(a)

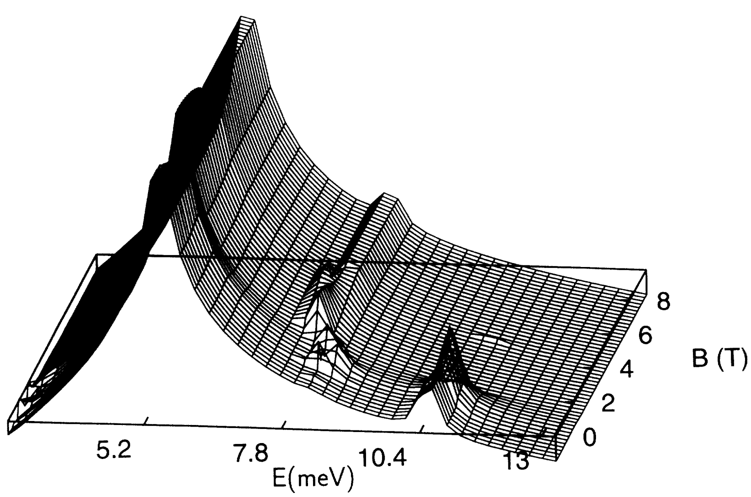

(b)

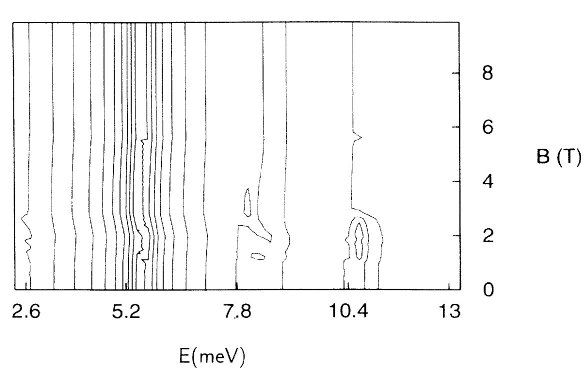

(c)

FIG. 7. Same as Fig. 5 with $f = 0.6$.

$$R(E_{\text{phot}}) \propto \frac{1}{E_{\text{phot}}} \sum_{i,n,m,s} F(E_a - E_{i,n,s} + E_{\text{phot}}) \times \left| \langle a|\hat{\mathbf{P}} \cdot \boldsymbol{\epsilon}|i,n,m,s\rangle \right|^2 . \quad (15)$$

We have not considered the many-body electronic interactions (the "Fermi-edge singularities") that can enhance the luminescence spectrum as states cross the Fermi energy.[28]

The acceptor state in the quantum well is calculated by a variational approximation, including the effects of the screened impurity potential, the quantum well potential, and the magnetic field. Because this is a wide quantum well with a shallow curvature in the valence band as well as the conduction band, the impurity potential is, by far, the most important energy in the bound state problem and will dominate the physics of the acceptor state. We use a Gaussian form for the bound state,

$$\Psi_a(\rho, z) = Ae^{-\frac{1}{2}(\alpha^2\rho^2 + \beta^2 z^2)}. \quad (16)$$

z is the growth direction of the well and the direction of the external magnetic field and ρ is the radial coordinate in the x-y plane. The energy of the bound hole is minimized with respect to α and β to get the form for the wave function. The resultant wave function is very close to that of the 3D acceptor state without the magnetic field and parabolic well.

The electron states are calculated from the self-consistent solutions of Schrödinger's equation. For the x-y dependence of the electron states we use the symmetric gauge because of the cylindrical symmetry of the problem. In this gauge, the electronic conduction band states in the x-y plane have the form

$$\psi_{n,m}(\rho, \phi) = \frac{C}{\sqrt{n!m!}} e^{-\rho^2/(2l^2)} e^{i(n-m)\phi} \times \sum_{j=0}^{\min(n,m)} (-1)^j \frac{n!m!}{j!(n-j)!(m-j)!} \times \left(\frac{\rho}{l}\right)^{n+m-2j}, \quad (17)$$

where ϕ is the angular coordinate in the x-y plane, $l = \sqrt{\frac{\hbar c}{eB}}$ is the magnetic length, n is the energy index of the Landau level [$E_n = \hbar\omega_c(n + 1/2)$], and m is the degeneracy index for the Landau level. The matrix elements in Eq. (15) are calculated using the expressions above for the electron and acceptor states and the symmetry of the Bloch states of the conduction and valence bands.

The polarization of the luminescence can be used to distinguish between the two electron spin states.[29] Because the lowest energy acceptor state is heavy-hole in nature,[30] the Bloch state of the hole in the transition has orbital angular momentum $L = 1$ with total z angular momentum $m_J = \pm 3/2$. Because the acceptor state is tightly bound at $\rho = 0$, and the electron states are of the form $\psi_{n,m} \propto (\rho/l)^{|n-m|}$ for small ρ, only the states $\psi_{n,n}$ have significant overlap with the acceptor state. These states have orbital z angular momentum $L_z = 0$ and total z angular momentum $m_J = \pm 1/2$ so that the resultant luminescence is, approximately, circularly polarized. Specifically, the $s = 1/2$ electrons will make transitions to the $m_J = 3/2$ hole states with polarization $\epsilon = \epsilon_+ = x + iy$ and the $s = -1/2$ electrons will make transitions to the $m_J = -3/2$ hole states with polarization $\epsilon = \epsilon_- = x - iy$. Therefore, distinguishing the polarization of the output luminescence will separate the spin-up and spin-down populations of electrons, and will enable the experimental observation of spin-dependent effects. This polarization is not exact due to the overlap between the acceptor state and states other than $\psi_{n,n}$. This is, however, a very good approximation because the binding length of the acceptor state is much smaller than the magnetic length, $1/\alpha \ll l$. In this case, $1/\alpha \approx 20$ Å and $l \geq 100$ Å.

In Fig. 8, we show a contour plot of the luminescence

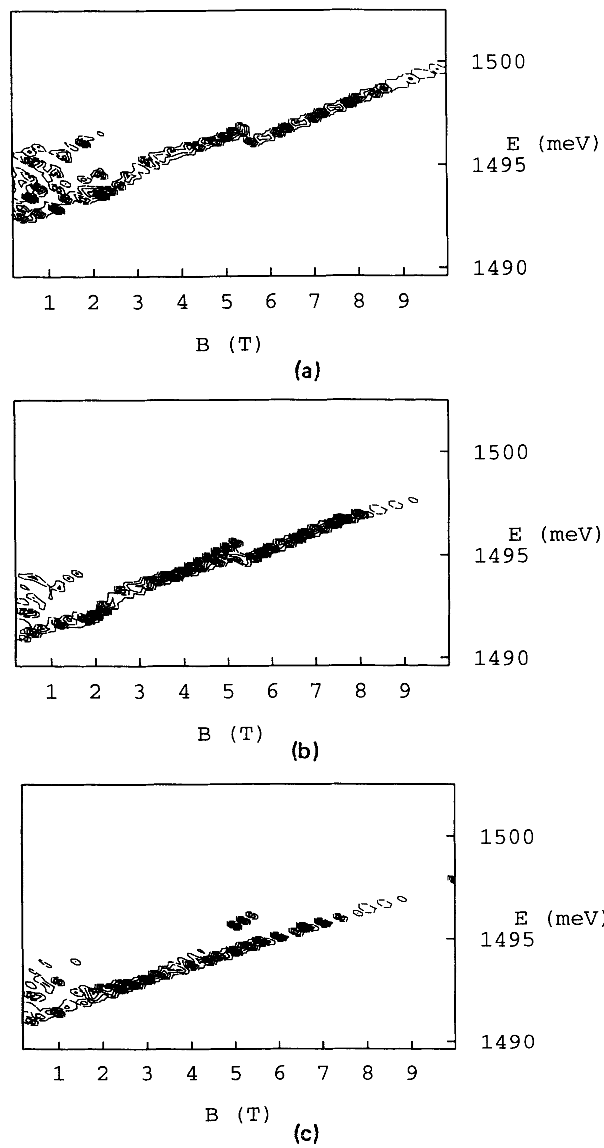

FIG. 8. Acceptor photoluminescence as a function of photon energy and magnetic field for a parabolic well, $w = 1000$ Å and $n_3 = 2 \times 10^{16}$ cm^{-3}. (a) $f = 1.0$, (b) $f = 0.8$, (c) $f = 0.6$.

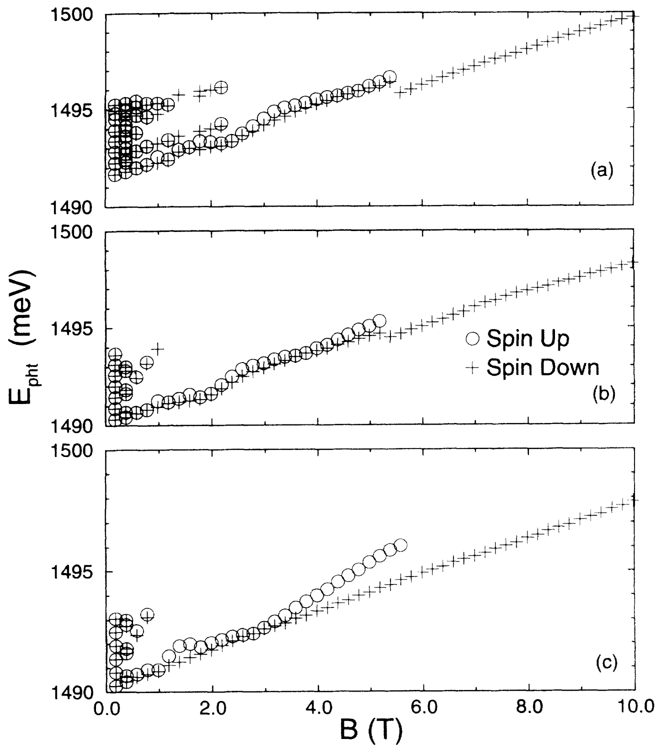

FIG. 9. Peaks in the acceptor photoluminescence as a function of magnetic field for the well described in Fig. 8 with (a) $f = 1.0$, (b) $f = 0.8$, (c) $f = 0.6$. Spin-up electrons marked by (o) and spin-down electrons marked by (+).

spectrum from a parabolic quantum well as a function of the magnetic field (x axis) and photon energy (y axis). We have used the same well parameters as in Sec. III above, with filling factors 1.0, 0.8, 0.6 plotted in Figs. 8(a), 8(b), and 8(c), respectively. We see the luminescence follows closely the subband spectra plotted in Figs. 5(a), 6(a), and 7(a). At low magnetic fields there are several populated Landau levels for each subband, giving a broad luminescence band. At higher fields, we find distinct signatures of populated subbands, nonlinearities of the subband energies due to subband depopulation, and distinct features of the spin polarization around 5.5 T. The width of these lines is due to the broadening of the density of states. Broadening due to experimental apparatus is not included.

The spin dependence of the electron states can be observed through the polarization of the emitted photons. In Fig. 9, we have plotted the positions of peaks in the luminescence as a function of the magnetic field for each spin. Figures 9(a), 9(b), and 9(c) are for filling factors 1.0, 0.8, and 0.6, respectively. One should note that there is no signal from the second subband due to the fact that it has zero amplitude at the well center. Higher energy peaks at low magnetic fields, particularly for filling factors 0.8 and 0.6 are due to higher Landau levels of the lowest subband. These figures show quite clearly the subband level spectrum for the wide parabolic well. We see the nonlinear behavior of the subbands with increasing magnetic field, and the enhanced spin splitting of the levels predicted previously.[14] At higher magnetic field, we see the abrupt end of one spin population due to the spin polarization of the electron gas. This will result, experimentally, in the abrupt polarization of the emitted luminescence and shift in the photon energy due to the change in the electron states. This is another clear indication of the predicted spin polarization of the electrons.

V. CONCLUSIONS

We have used numerical studies of wide parabolic quantum wells to determine experimental signatures of electron-electron interaction and spin effects in these wells. We have seen important correlation and spin dependence in the magnetotransport, and signatures of the electron density distribution and spin population in optical experiments. For the integer quantum Hall effect in these wells, the spin splitting of levels is important to understand the observed disappearance and reappearance of Hall plateaus as the density of the electron gas changes. There is also a possibility of detecting spin polarization in Shubnikov–de Haas experiments. Infrared absorption in these wells displays satellite peaks above the 3D plasma mode that show strong dependence on the electron spin. Finally, we propose acceptor photoluminescence experiments as an ideal probe of the subband spectrum and many-body effects. We see that enhanced spin splitting and spin polarization should be observable in experimental investigations. These results are in qualitative agreement with excitonic luminescence data.

ACKNOWLEDGMENTS

This research was supported, in part, by the National Science Foundation through Grant No. DMR-8922222 and the ARO through Grant No. DAAL03-91-G-0049.

[1] M. Shayegan, T. Sajoto, M. Santos, and C. Silvestre, Appl. Phys. Lett. **53**, 791 (1988); T. Sajoto, J. Jo, L. Engel, M. Santos, and M. Shayegan, Phys. Rev. B **39**, 10 464 (1989); M. Sundaram, A. C. Gossard, J. H. English, and R. M. Westervelt, Superlatt. Mictrostruct. **4**, 683 (1988); E. G. Gwinn, R. M. Westervelt, P. F. Hopkins, A. J. Rimberg, M. Sundaram, and A. C. Gossard, Phys. Rev. B **39**, 6260 (1989); M. Sundaram, A. C. Gossard, and P. O. Holtz, J. Appl. Phys. **69**, 2370 (1991).

[2] M. Shayegan, T. Sajoto, J. Jo, M. Santos, and H. D. Drew, Phys. Rev. B **40**, 3476 (1989).

[3] E. G. Gwinn, R. M. Westervelt, P. F. Hopkins, A. J. Rimberg, M. Sundarum, and A. C. Gossard, Phys. Rev. B **39**, 6260 (1989).

[4] K. Ensslin, M. Sundaram, A. Wixforth, J. H. English, and A. C. Gossard, Phys. Rev. B **43**, 9988 (1991); K. Ensslin, A. Wixforth, M. Sundararam, P. F. Hopkins, J. H. English, and A.C. Gossard, *ibid.* **47**, 1366 (1993).

[5] K. Karrai, M. Stopa, X. Ying, H. D. Drew, S. Das Sarma, and M. Shayegan, Phys. Rev. B **42**, 9732 (1990).

[6] K. Karrai, X. Ying, H. D. Drew, M. Santos, M. Shayegan, S. R. E. Yang, and A. H. MacDonald, Phys. Rev. Lett. **67**, 3428 (1991).

[7] L. Brey, N. F. Johnson, and B. I. Halperin, Phys. Rev. B **40**, 10 647 (1989); L. Brey and B. I. Halperin, *ibid.* **40**, 11 634 (1989).

[8] A. Wixforth, M. Sundaram, K. Ensslin, J. H. English, and A. C. Gossard, Appl. Phys. Lett. **56**, 454 (1990); A. J. Rimberg, Scott Yang, Jed Dempsey, J. H. Baskey, R. M. Westervelt, M. Sundaram, and A. C. Gossard, *ibid.* **62**, 390 (1993); J. Jo, E. A. Garcia, K. M. Abkemeier, M. B. Santos, and M. Shayegan, Phys. Rev. B **47**, 4056 (1993).

[9] M. Fritze, W. Chen, A. V. Nurmikko, J. Jo, M. Santos, and M. Shayegan, Phys. Rev. B **45**, 8408 (1992); J. H. Burnett, H. M. Cheong, W. Paul, P. F. Hopkins, and A. C. Gossard, *ibid.* **48**, 7940 (1993).

[10] M. P. Stopa and S. Das Sarma, Phys. Rev. B **40**, 10 048 (1989); **45**, 8526 (1992); **47**, 2122 (1993).

[11] L. Brey, Phys. Rev. B **44**, 3772 (1991).

[12] A. J. Rimberg and R. M. Westervelt, Phys. Rev. B **40**, 3970 (1989).

[13] C. E. Hembree, B. A. Mason, A. Zhang, and J. A. Slinkman, Phys. Rev. B **46**, 7588 (1992).

[14] C. E. Hembree, B. A. Mason, J. T. Kwiatkowski, J. Furneaux, and J. A. Slinkman, Phys. Rev. B **48**, 9162 (1993).

[15] O. Gunnarsson and B. I. Lundqvist, Phys. Rev. B **13**, 4274 (1976).

[16] L. Hedin and B. I. Lundquist, J. Phys. C **4**, 2064 (1971).

[17] Frank Stern and Sankar Das Sarma, Phys. Rev. B **30**, 840 (1984).

[18] T. Ando, J. Phys. Soc. Jpn. **37**, 622 (1974); **37**, 1233 (1947).

[19] A. Ishihara and L. Smrcka, J. Phys. C **19**, 6777 (1986).

[20] K. Karrai, H. D. Drew, M. W. Lee, and M. Shayegan, Phys. Rev. B **39**, 1426 (1989).

[21] Achim Wixforth, M. Sundaram, J. H. English, and A. C. Gossard, in *Proceedings of the 20th International Conference on the Physics of Semiconductors*, edited by E. M. Anastassakis and J. D. Joannopoulus (World Scientific, Singapore, 1990), p. 1705; A. Wixforth, M. Sundaram, K. Ensslin, J. H. English, and A. C. Gossard, Phys. Rev. B **43**, 10 000 (1991).

[22] L. Brey, J. Dempsey, N. F. Johnson, and B. I. Halperin, Phys. Rev B **42**, 1240 (1990).

[23] L. Brey, N. F. Johnson, and J Dempsey, Phys. Rev. B **42**, 2886 (1990).

[24] J. Jo, M. Santos, M. Shayegan, Y. W. Suen, and L. W. Engel, Appl. Phys. Lett. **57**, 2130 (1990).

[25] Jed Dempsey and B. I. Halperin, Phys. Rev. B **45**, 1719 (1992).

[26] Jed Dempsey and B. I. Halperin, Phys. Rev. B **47**, 4662 (1993); **47**, 4674 (1993).

[27] T. Ando, Z. Phys. B **24**, 33 (1976); J. Phys. Soc. Jpn. **44**, 475 (1978); Phys. Rev. B **19**, 2106 (1979).

[28] Pawel Hawrylak, Phys. Rev. B **42**, 8986 (1990); **44**, 11 436 (1991); **45**, 4237 (1992).

[29] B. P. Zakharchenya, D. N. Mirlin, V. I. Perel', and I. I. Reshina, Usp. Fiz. Nauk **136**, 459 (1982) [Sov. Phys. Usp. **25**, 143 (1982)].

[30] D. J. Ashen, P. J. Dean, D. T. J. Hurle, J. B. Mullin, A. M. White, and P. D. Greene, J. Phys. Chem. Solids **36**, 1041 (1975); A. Baldereschi and Nunzio O. Lipari, Phys. Rev. B **8**, 2697 (1973).

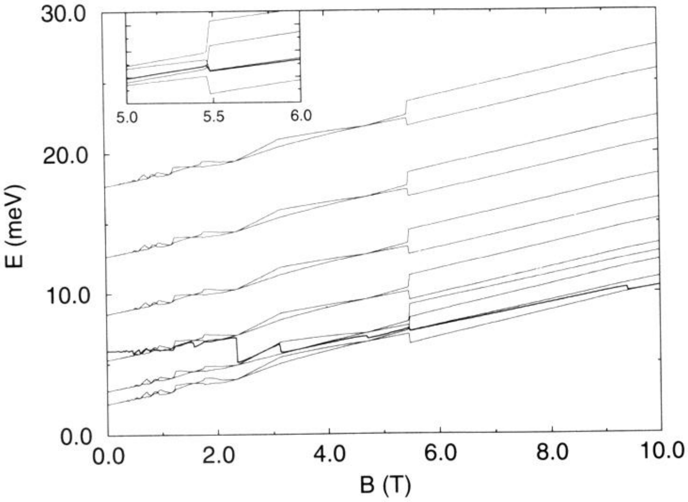

(a)

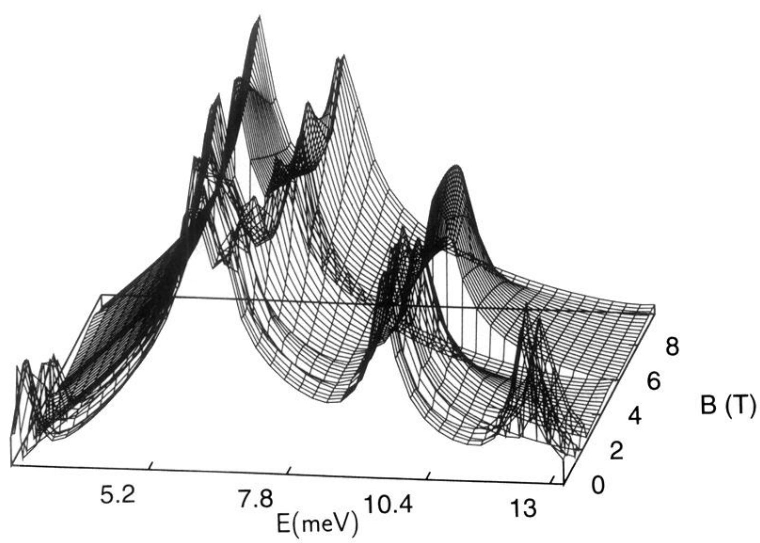

(b)

FIG. 5. Infrared optical absorption spectrum of a wide parabolic well, $w = 1000$ Å and $n_3 = 2 \times 10^{16}$ cm^{-3} at $f = 1.0$. (a) Subband spectrum as a function of magnetic field, (b) $\log_{10} \sigma_{xx}(\omega)$ as a function of energy and magnetic field, (c) Contour plot of $\log_{10} \sigma_{xx}(\omega)$.

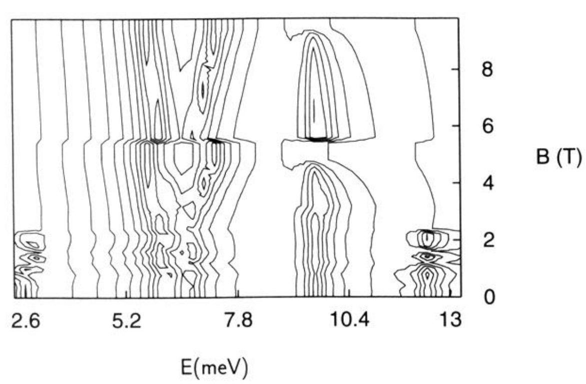

(c)

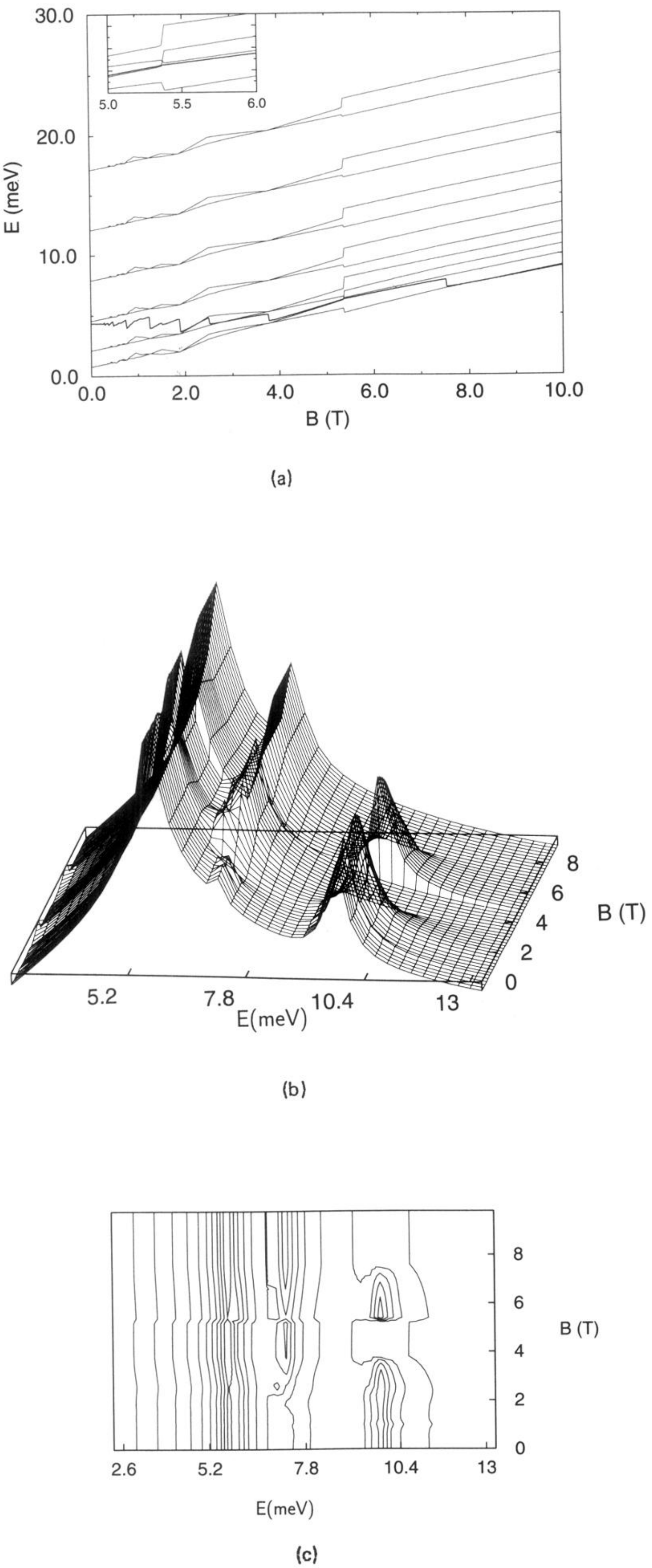

FIG. 6. Same as Fig. 5 with $f = 0.8$.

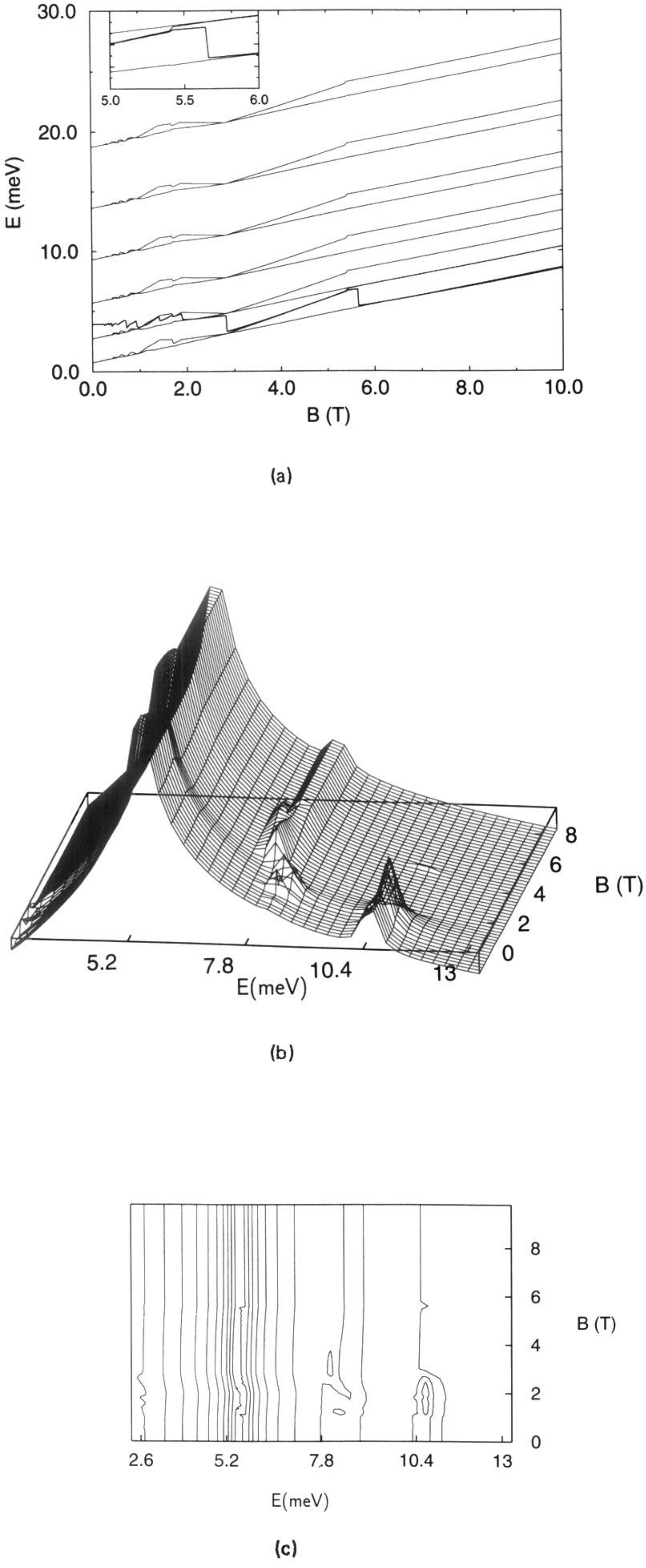

FIG. 7. Same as Fig. 5 with $f = 0.6$.